Proceedings World Geothermal Congress 2023
Beijing, China, April 17 – 21, 2023

Changes in Hydraulic Properties of the Geothermal Fracture Induced by Cyclic Loading-unloading Processes

Yilong Yuan [a, b, *], Chenghao Zhong [a], Tianfu Xu [a, b], Fabrizio Gherardi [a, c]

[a] Key Laboratory of Groundwater Resources and Environment Ministry of Education, Jilin University, Changchun 130021, China

[b] Engineering Research Center of Geothermal Resources Development Technology and Equipment, Ministry of Education, Jilin University, Changchun 130026, China

[c] Istituto di Geoscienze e Georisorse (IGG), Consiglio Nazionale delle Ricerche (CNR), 56124 Pisa, Italy

yuanyl14@mails.jlu.edu.cn

Keywords: Enhanced geothermal system; Geothermal fracture; Mechanical deformation; Fracture permeability; Granite

ABSTRACT

Sustainable and profitable energy production from the enhanced geothermal system (EGS) requires a comprehensive understanding of the coupled effects of elastic and plastic deformation on the hydraulic evolution (e.g., fracture aperture, permeability and conductivity) of geothermal fracture. In this work, four flow-through tests were conducted on granite samples with a rough single fracture at 25-180℃. Each test was performed on three cycles of loading-unloading processes within a confining pressure of 5-30 MPa. Experimental results indicated that the hydraulic properties are negatively correlated with confining pressure in a logarithmic manner. The coupled effects of elastic and plastic deformation induced by stress loading are the main factor affecting fracture hydraulic properties. Plastic deformation is associated with the mineral grains crush that occurs in fracture contacting asperities, which is a permanent and irreversible process. Compared to the results at 25℃, a larger reduction in permeability is observed at 180℃, as revealed by a maximum reduction in hydraulic aperture up to more than 40% at this temperature. This means that larger plastic deformations in the fractures are associated with higher temperatures. Therefore, the addition of proppant is very important for sustainable geothermal development for fractured geothermal reservoirs under high-stress conditions. The free-face dissolution was well confirmed by ion concentration detection from the effluent solution, which is beneficial for the low permeability geothermal reservoir due to its positive effect on fracture hydraulic properties, especially for the high-temperature geothermal fractures. As the number of loading-unloading cycles increases, the hysteresis effect induced by plastic deformation becomes less and less according to the cyclic test. Compared to the first loading-unloading stage, the maximum decline of permeability decreases from 73% to 6% and 1% on the second and third stages, respectively. However, pressure dissolution under the long-term stress loading should be further discussed, because it may disrupt the self-propping balance of geothermal fracture asperities.

1. INTRODUCTION

One of the greatest challenges of the twenty-first century is mitigating climate change and greenhouse effects in conjunction with uptrend energy demand (George, Shen et al. 2021). The global total energy demand is expected to increase more than a third by 2035, requiring about a 77% increase in renewable resources (Usman, Khalid et al. 2021). Geothermal energy, one of the most promising low-carbon resources to alleviate climate change, attracts significant attention from scientists and decision-makers.

Hot dry rock (HDR) geothermal energy is stored in low porosity, low permeability, and high temperature (over 150 ℃) crystalline rock at a depth of 3 to 10 km (Lu 2018). The HDR geothermal energy in China exceeds 2.52×10^{25} J, which can provide energy for 3945 years if 2% of that is exploited (Hao, Fei et al. 2015). The HDR consists of two main categories (ERDA 1977): (1) conduction- and radiogenic-related HDR in the crust and (2) igneous-related HDR. Noteworthy, abundant igneous-related HDR resources have been found in the Gonghe Basin, northeastern Tibetan Plateau, China (Zhang, Hu et al. 2020).

Since the 1970s, enhanced geothermal system (EGS) has provided a pathway to efficiently and economically utilize the HDR geothermal energy (Olasolo, Juárez et al. 2016). The EGS harvests heat energy by circulating working fluids in an artificial fractured reservoir through injectors and producers (Zhong, Xu et al. 2022). A successful EGS extensively employs hydraulic fracturing to obtain intricate fracture networks. Hydraulic fracturing uses pressurized fluid to initiate and propagate artificial fractures, thereby enhancing the permeability of geothermal reservoirs (Li, Pan et al. 2015). Fractures typically have higher permeability compared to the surrounding rock matrix, even when the confining pressure reaches 100 MPa (Watanabe, Hirano et al. 2006). Therefore, fractures act as main flow conduits in EGS reservoirs. Generally, the permeability of the fracture network is closely related to the production performance of the EGS plant (Fang, Wang et al. 2017).

Fluid flow through a geothermal fracture is a Thermal-Hydraulic-Mechanical-Chemical (THMC) coupling process (Yasuhara, Polak et al. 2006). Compared to the porous medium, fluid transport within a fractured medium is more complex and significantly affected by THMC coupled processes (Polak, Elsworth et al. 2003, Rabczuk and Belytschko 2004, Ghassemi and Zhang 2006, Zhou, Zhuang et al. 2018). It is crucial for EGS engineering to understand the THMC coupled effects on the transient changes of the geothermal fracture permeability.

Before investigating more complicated field-scale fracture networks, we should first understand the behavior of fluids in individual fractures. Hofmann, Blöcher et al. (2016) illuminated the hydraulic and elastic behaviors in granitic fracture rocks during two cyclic loading-unloading. Vogler, Amann et al. (2016) studied the role of mated/unmated rough surfaces in fracture permeability reduction during single cyclic loading-unloading. Zhao, Wang et al. (2020) investigated the elastoplastic contact of asperity in fracture surfaces

during the unloading process. Shu, Zhu et al. (2020) investigated the permeability evolution of a single granite fracture at 100~200 ℃ consistent with realistic EGS reservoir temperature conditions. These studies are of great significance to reveal the evolution of geothermal fracture permeability. However, most of these studies only consider the effect of elastic deformation on the geothermal fracture under the single loading-unloading process. In addition, the experimental confining pressure was relatively low (e.g., <20 MPa) because of the difficulty of sealing at high temperatures. As a result, the potential effects induced by plastic deformation on the geothermal fracture are inadvertently overlooked, especially under the high confining pressure and the multiple cycles of loading-unloading processes. Moreover, the water and rock reactions have rarely been analyzed before to identify the geochemistry effects, while only the combined effects of permeability changes are analyzed in previous studies.

To fill the above research gap, a series of flow-through experiments are conducted on the fractured granite samples under multiple cycles of loading-unloading, to fully investigate the coupled effects of elastic and plastic deformation on the geothermal fracture evolution. The maximum temperature and confining pressure reach 180 ℃ and 30 MPa, respectively. The aqueous solution after the flow-through test is collected to analyze the strength of the water-rock reaction under different temperature and confining pressure conditions. This is very important to identify the coupled effects of mechanical deformation on geothermal fracture. The novelty of this work is highlighted in three aspects: 1) revealing the hydraulic evolution of rough granite fracture under multiple cycles of loading-unloading; 2) simulating the real temperature and in-situ stress of the deep geothermal reservoir; 3) clarifying the essential mechanisms responsible for the geothermal fracture evolution. The results presented in this work are very beneficial to supporting the development of geothermal energy and oil/gas fractured reservoirs.

2. EXPERIMENTAL METHODS

2.1 Rock sample preparation

Fig. 1a shows the tested cylindrical granite specimens with a diameter of 25 mm and a length of 50 mm, which were collected from the outcrops in the Gonghe Basin, Qinghai Province, China. The Gonghe Basin is a promising region for EGS exploitation in China (Xu, Yuan et al. 2018). Initially, we polished the surface of the samples with sandpaper to protect the gum sleeve (**Fig. 1a**). The rock samples were split into two halves using the Brazilian split method. As shown in **Fig. 1b**, the granite cores were fixed in a uniaxial compressive apparatus and loaded with compressive stress by two sharp wedges. As a result, the cylindrical sample with an artificial rough fracture could be obtained to conduct the flow-through tests. In this work, four tested samples were prepared to investigate the effect of temperature on the geothermal fracture evolution (**Fig. 1c**).

According to the scanning electron microscope (SEM), the granitic samples are medium-grained (2~5 mm) with massive structure. The granite samples contain large traces of plagioclase (42%) and quartz (30%), minor traces of K-feldspar (18%), biotite (8%), and other minerals (2%).

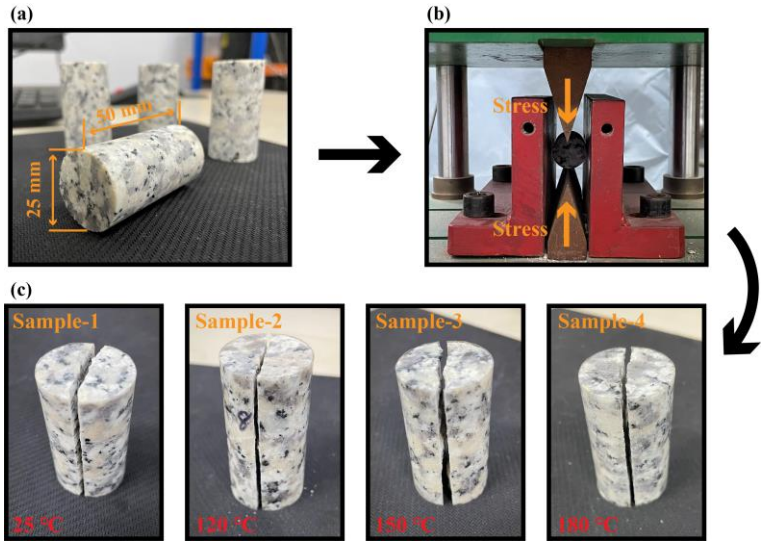

Figure 1: Granite specimen preparation: (a) the cylindrical samples before Brazilian split, (b) the Brazilian split setup, and (c) four fracture samples after Brazilian split.

2.2. Experiment system

Fig. 2 shows the custom-designed experiment system which was manufactured by Nantong Huaxing Petroleum Instrument Co., Ltd (Jiangsu Province, China). The experiment system is suitable for conducting hydraulic evolution tests. It contains five main parts: injection, core holder, confining pressure, heating, and data acquisition and recording systems. The injection pump with a maximum injection pressure of 40 MPa is manufactured by Teledyne ISCO, USA (**Fig. 2c**). The granite samples were fixed in the core holder (**Fig. 2b**), which was placed horizontally inside the heating box (**Fig. 2a**). Noteworthy, the sample was wrapped within a thin layer of polymer waterproof tape prior to installation into the core holder, ensuring fluid flows only in the artificial fracture (**Fig. 2b**). Driven by a hand pump, water was pumped to the part between the gum sleeve and the core holder, thus controlling confining pressure (the upper limit is 30 MPa). The core holder was settled in the heating box which is devoted to the heating systems. The upper-temperature limit of the heating box is 180 ℃. Data acquisition and recording systems were used to record the inlet and outlet pressure, flow rate, and time during the flow-through tests. In addition, a condenser is installed at the outlet to facilitate high-temperature experimental sampling.

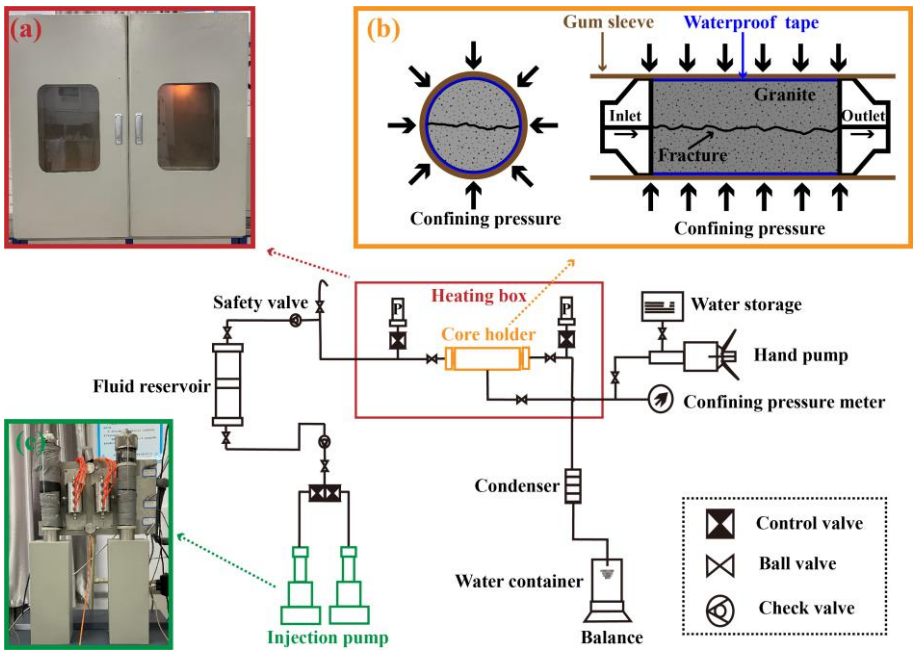

Figure 2: Experiment system of the flow-through tests.

2.3. Experimental procedure

Four individual tests were conducted at the normal temperature scenario (25 ℃) and the high-temperature scenarios (120 ℃, 150 ℃, and 180 ℃), respectively. The rock samples were maintained at the specified temperature before the test started. **Fig. 3** displays the schematic diagram of the confining pressure cyclic loading-unloading path. The confining pressure gradually increases from 5 MPa to 30 MPa in each loading stage, and then gradually decreases along the original path in each unloading stage. Distilled water was used as a working fluid during the test, thus any element concentrations observed in the effluent were caused by the dissolution of the minerals from the fracture surface. The input water was deposited in a buffer tank before entering rock samples. The buffer tank was placed in an incubator and maintained at the same value as the rock temperature. Therefore, the actual input fluid temperature in the experiment is the same value as the rock temperature. A constant back pressure of 1MPa was set in each experimental scheme to ensure that the water could remain liquid at high temperatures (e.g., 180°C). Furthermore, the injection flow rate was maintained at a constant value of 5 ml/min in each scenario. The injection pressure was monitored and recorded every 60 seconds during the flow-through experiments.

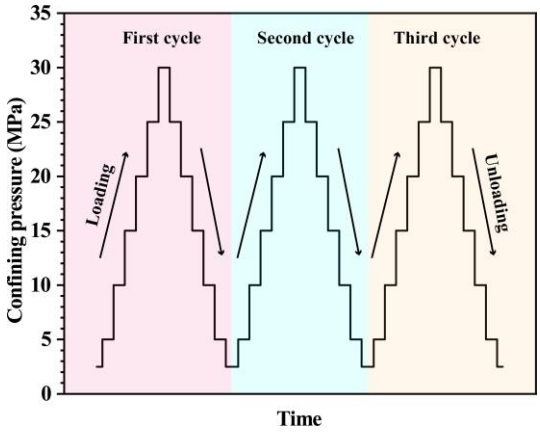

Figure 3: Schematic diagram of the cyclic loading-unloading processes.

2.4. Methods of calculation

The simplified Navier-Stokes equations (Zimmerman and Bodvarsson 1996) represent a rock fracture consisting of two smooth plates with constant aperture, which are widely used to describe Newtonian viscous fluid flow through a single fracture (Liu, Li et al. 2016). When the fluid remains laminar in the fracture at a low velocity, the velocity component perpendicular to the fracture plane can be essentially negligible. Hence, the modified Cubic law (Witherspoon, Wang et al. 1980) is introduced to estimate the equivalent fracture aperture b_e of the rough fracture samples based on simplified Navier-Stokes equations. The calculation of b_e as shown in Eq. **Fehler! Verweisquelle konnte nicht gefunden werden.**.

$$b_e = \sqrt[3]{\frac{12\mu qL}{Pd}} \tag{1}$$

where q is the flow rate (m^3/s); P is the water pressure difference between inlet and outlet (Pa); μ is the dynamic viscosity of water (Pa·s); d and L are width and length of the fracture (m), respectively. The effectiveness of the Eq. (1) for the rough fracture has been well proved by previous studies (Shu, Zhu et al. 2019, Huang, Zhang et al. 2021).

Based on the measured pressure difference P, the permeability k_e of a single fracture can be calculated using Darcy's law (Caulk, Ghazanfari et al. 2016), as shown in Eq. **Fehler! Verweisquelle konnte nicht gefunden werden.**.

$$k_e = \frac{q \cdot \mu \cdot L}{P \cdot A} \tag{2}$$

where A is the cross-sectional area of fracture (m^2), which is equivalent to multiply b_e by L. In this work, the dynamic viscosity μ and density ρ of water following temperatures.

According to Eqs. **Fehler! Verweisquelle konnte nicht gefunden werden.** and **Fehler! Verweisquelle konnte nicht gefunden werden.**, as postulating the permeability of the rock matrix is negligibly small, the formula for the permeability of a single fracture can be obtained as follow:

$$k_e = \frac{b_e^2}{12} \tag{3}$$

The hydraulic conductivity K (Shu, Zhu et al. 2020) expresses the flow rate of water per unit hydraulic gradient, which is related to the properties of fluid and rock, as defined by Eq. (4). A higher K value manifests the fluid flows faster in the fracture.

$$K = \frac{k_e \cdot g \cdot \rho}{\mu} \tag{4}$$

where g is the gravitational acceleration (9.8 m^2/s).

3. RESULTS ANALYSIS AND DISCUSSION

3.1 Effect of mechanical deformation on hydraulic properties

The inability to systematically isolate and control for differences between samples (e.g., fractured asperity) makes it difficult to intuitively compare the hydraulic properties of each test. Therefore, similar to the analysis of Shu, Zhu et al. (2020), we calculated the ratios of hydraulic aperture and permeability relative to their initial value at 5 MPa in 25 ℃, as shown in **Fig. 4**. According to Eq. **Fehler! Verweisquelle konnte nicht gefunden werden.**, the curve trending of the permeability is similar to that of the hydraulic aperture, but it shows more drastic changes than that of the hydraulic aperture because of the exponential relationship in fracture permeability.

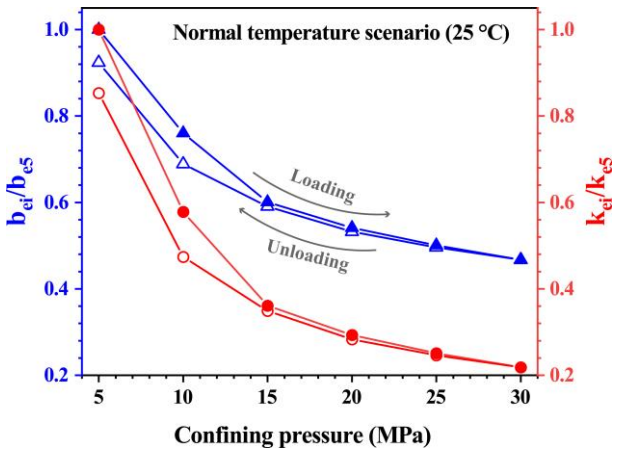

Figure 4: Evolutions of the normalized hydraulic aperture b_{ei}/b_{e5} and permeability k_{ei}/k_{e5} in the first loading-unloading stage at 25 ℃.

During the loading stage, the normalized hydraulic aperture and permeability are continuously reducing with confining pressure in a logarithmic manner. The normalized hydraulic aperture and permeability reduce faster during the early loading stage because the pressure significantly affects the fracture asperities. As the confining pressure increases from 5 to 30 MPa, the normalized hydraulic aperture and permeability decreased by 53% and 78%, respectively.

During the unloading stage, the normalized hydraulic aperture and permeability are continuously increasing with confining pressure in a logarithmic manner. This recovery process is mainly controlled by the elastic deformation of fracture. However, the hydraulic properties cannot be completely restored to the initial value, even when the confining pressure decreases to the original value of 5 MPa (**Fig. 4**). As the confining pressure decreases from 30 to 5 MPa, the normalized hydraulic aperture and permeability increase by 45% and 63%, respectively. This hysteretic effect of hydraulic properties is mainly controlled by the plastic deformation, which is a permanent and irreversible process (Hofmann, Blöcher et al. 2016).

Plastic deformation is usually associated with the mineral grains crush that occurs in the fracture contacting asperities, as shown in **Fig. 5**. This process is also coupled with the fall off mineral grains (Siratovich, Villeneuve et al. 2015). In addition, some mineral grains larger than the fracture aperture are retained in the fracture, thus further blocking the flow spaces. The test results show that

the coupled effects of elastic and plastic deformation induced by stress loading is the main factor affecting fracture hydraulic properties (Yasuhara, Elsworth et al. 2004, Ghassemi and Suresh Kumar 2007, Yasuhara and Elsworth 2008, Yasuhara, Kinoshita et al. 2011).

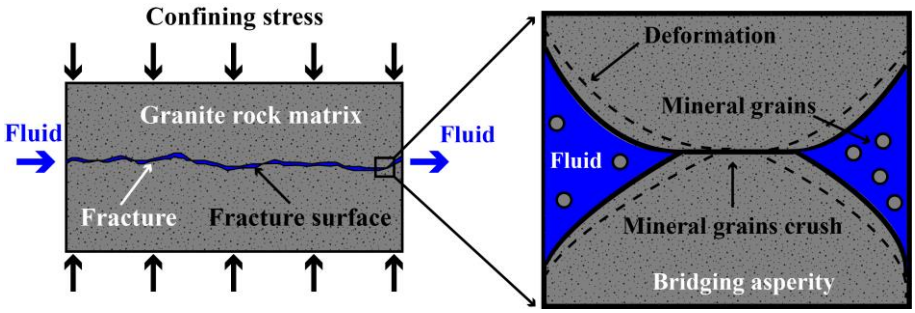

Figure 5: Schematic diagram of mechanical deformation effects on fracture at 25 ℃. The dashed line refers to the fracture surface before deformation.

3.2 Effect of temperature on hydraulic properties

EGS plants extract thermal energy from the hot rock matrix by injecting a cool working fluid through geothermal fractures. Synchronously, thermal and pressure system imbalance occurs in fractured reservoirs. According to the real temperature of deep geothermal reservoirs, three individual high-temperature tests (120 ℃, 150 ℃, and 180 ℃) were conducted to investigate the effect of temperature on fracture hydraulic properties. Similar to the previous analyses, we calculated the ratios of hydraulic aperture and permeability relative to their initial value at 5 MPa, as shown in **Fig. 6**.

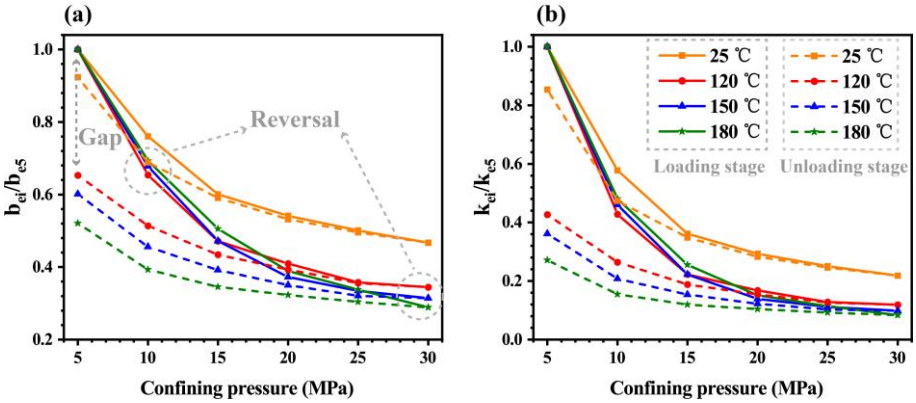

Figure 6: Evolutions of the normalized (a) hydraulic aperture b_{ei}/b_{e5} and (b) permeability k_{ei}/k_{e5} in the first loading-unloading stage at different temperature conditions.

During the loading stage, the hydraulic aperture decreases by 66%, 69% and 71%, the permeability decreases by 88%, 90% and 92%, at 120, 150 and 180 ℃, respectively. The test results indicate that the normalized hydraulic aperture and permeability decrease more sharply at higher temperature scenarios. During the unloading stage, the hydraulic aperture increases by 31%, 29% and 23%, the permeability increases by 31%, 26% and 19%, at 120, 150 and 180 ℃, respectively. This shows that elastic deformation recovery slowly decreases with increasing temperature.

The gap index is used to quantitatively assess the impact of temperature, which is defined as the difference in normalized hydraulic properties between the loading and unloading stages. **Fig. 7** shows the evolutions of hydraulic aperture gap and permeability gap with confining pressures at different temperature conditions. These curves show similar downtrends, indicating plastic deformation in the fracture is relatively weak at high confining pressures. In addition, the hydraulic gap increases with increasing temperature at arbitrary confining pressure. Compared to the 25 ℃ results, the maximum gaps (e.g., at 5 MPa) of hydraulic aperture and permeability increase from 8% and 15% to 48% and 73% at 180 ℃, respectively. These test results show that stronger coupled effects of elastic and plastic deformation occur on the geothermal fracture at higher temperatures. Therefore, for fractured geothermal reservoirs under high-stress conditions, the addition of proppant is very important for sustainable geothermal development (Lu 2018, Yuan, Xu et al. 2020).

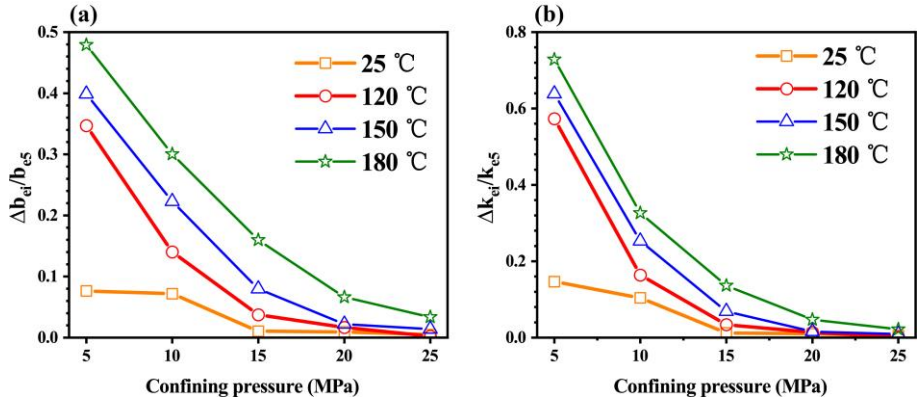

Figure 7: Evolutions of the (a) hydraulic aperture gap $\Delta b_{ei}/b_{e5}$ and (b) permeability gap $\Delta k_{ei}/k_{e5}$ with confining pressures at different temperature conditions.

3.3 Effect of cyclic loading-unloading on hydraulic properties

This section focuses on the coupled effects of elastic and plastic deformation on hydraulic properties in the geothermal fracture induced by multiple cycles of loading-unloading processes (see **Fig. 3**). **Fig. 8** shows the comparisons of hydraulic aperture gap and permeability gap at 5 MPa on three cycles of loading-unloading processes.

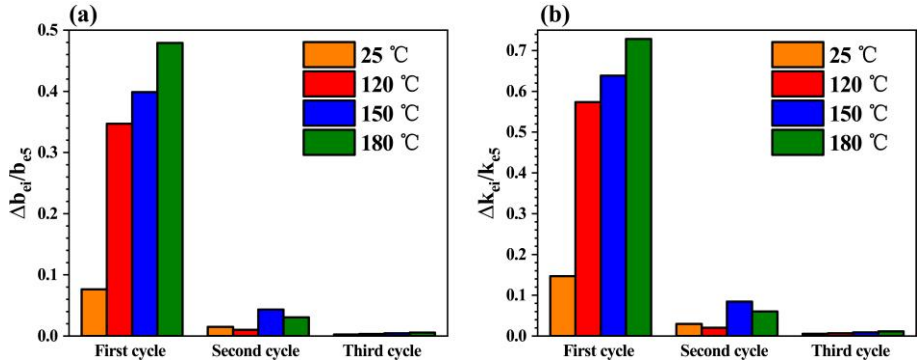

Figure 8: Comparisons of the (a) hydraulic aperture gap $\Delta b_{ei}/b_{e5}$ and (b) permeability gap $\Delta k_{ei}/k_{e5}$ at 5 MPa on three cycles of loading-unloading processes.

As shown in **Fig. 8**, the hysteresis effect is most significant in the first loading-unloading cycle. In addition, the hydraulic property gap basically increases with temperature during each loading-unloading stage. As the number of cycles increases, the hysteresis effect induced by plastic deformation becomes less and less. For example, at 180 ℃, the maximum permeability gap (e.g., at 5 MPa) decreases from 73% to 6% and 1% during the 2nd and 3rd loading-unloading stages, compared to that of the 1st stage.

This phenomenon can be illustrated by some additive processes in the multiple loading-unloading cycles, as shown in **Fig. 9**. The test conditions at low temperature of 25 ℃ (**Fig. 9a**) and high temperature of 180 ℃ (**Fig. 9b**) are taken as examples. Irreversible plastic deformation still exists in the 2nd and 3rd loading stages, because the mineral grains at contacting asperities may be further crushed. In addition, the mechanical properties of granite samples at high temperatures weaken with time (Peng, Zhao et al. 2020). The fracture may shrink and close with the decrease in granite strength (**Fig. 9b**). Consequently, the hydraulic aperture and permeability of fracture were further reduced.

Moreover, the free-face dissolution still exists and the pressure dissolution may occur during the cyclic loading-unloading processes (Zhou, Li et al. 2020). However, the free-face dissolution may play a limited role in the later loading-unloading stage, because of the significant reduction of fracture non-contacting surface. In addition, both types of dissolution will cause more chemical components to precipitate on the fracture surface with time (Shu, Zhu et al. 2020). As a result, the fracture aperture may be further reduced.

A review of **Fig. 8** indicates that the hysteresis effect is negligible (e.g., ≤1%) until at least three cycles of loading-unloading processes for the high-temperature geothermal fracture (e.g., ≥150℃). Therefore, it is more difficult to obtain stable fracture networks when the EGS plant is developed in geothermal reservoirs with high temperatures. The hydraulic properties of geothermal fractures tend to be temporarily stabilized after the loading-unloading processes. According to previous studies (Yasuhara, Elsworth et al. 2004, Yasuhara and Elsworth 2008, Watanabe, Saito et al. 2020), it is very crucial to understand the pressure dissolution because it may disrupt the self-propping balance of fracture asperities under long-term stress loading. This process will significantly reduce the fracture permeability (Hofmann, Blöcher et al. 2016).

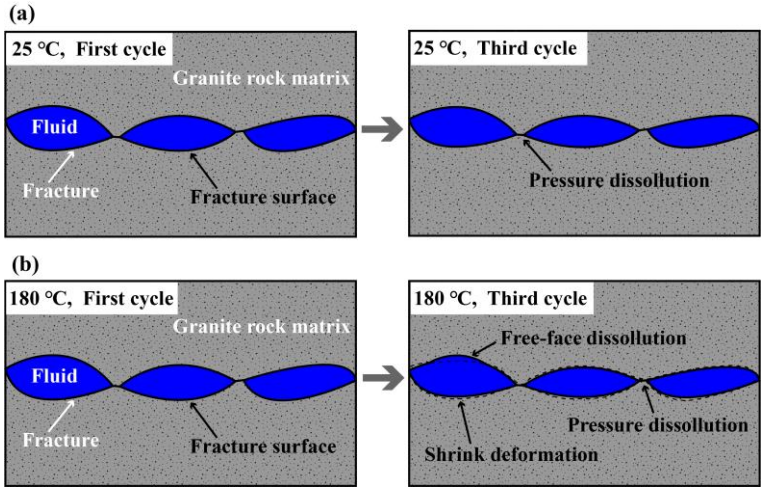

Figure 9: Schematic explanation of changes in hydraulic properties during cyclic loading-unloading processes. The dashed line refers to the fracture surface before the deformation.

4 CONCLUSION

Stable and high permeable fracture networks in the geothermal reservoir support sustainable and profitable energy production of the EGS. The mechanical deformation induced-by project operation (e.g., cold water injection, geothermal production, etc.) can greatly change the hydraulic properties of the geothermal fractures. In this work, a series of flow-through tests were conducted to investigate the coupled effects of elastic and plastic deformation on the hydraulic evolution of Brazilian-induced artificial granite fractures. The essential mechanisms responsible for the geothermal fracture evolution were well illuminated. Based on the flow-through tests, the following conclusions can be drawn:

(1) When the test temperature ranges from 25 ℃ to 180 ℃, the decrement of hydraulic aperture ranges from 53% to 71%, and permeability ranges from 78% to 92% during the 1st loading stage; the increment of hydraulic aperture ranges from 45% to 23% and permeability ranges from 63% to 19% during the 1st unloading stage. The test results show that the mechanical deformation of rough fracture induced-by stress loading is the main factor affecting fracture hydraulic properties. The hysteretic effect is observed, which is caused by the plastic deformation and becomes more pronounced at high temperatures.

(2) The effects of mechanical deformation under high temperatures result in the reversal phenomenon of hydraulic properties occurred as the confining pressure increases. This is because the increase of fracture permeability induced-by the free-face dissolution under high temperatures is gradually shown with the high confining pressure. These changes of free-face dissolution with temperature were well confirmed by ion concentration detection from the effluent solution.

(3) As the number of cycles increases, the hysteresis effect induced by plastic deformation becomes less and less. Compared to the 1st loading-unloading stage, the maximum fracture permeability decreases from 73% to 6% and 1% during the 2nd and 3rd stages at 180 ℃. According to the cyclic test, the plastic deformation can be neglected until at least three cycles of loading-unloading processes. For the specified test conditions of this work, the fracture hydraulic evolution may be affected by the fracture mechanical deformation, free-face dissolution, mineral grains rupture, and mineral grains blockage.

REFERENCES

Caulk, R. A., E. Ghazanfari, J. N. Perdrial and N. Perdrial (2016). "Experimental investigation of fracture aperture and permeability change within Enhanced Geothermal Systems." Geothermics **62**: 12-21.
ERDA (1977). Hot dry rock geothermal energy: status of exploration and assessment. Report No. 1 of the hot dry rock assessment panel, Energy Research and Development Administration, Washington, D.C. (USA)**:** 219.
Fang, Y., C. Wang, D. Elsworth and T. Ishibashi (2017). "Seismicity-permeability coupling in the behavior of gas shales, CO2 storage and deep geothermal energy." Geomechanics and geophysics for geo-energy and geo-resources. **3**(2): 189-198.
George, A., B. Shen, M. Craven, Y. Wang, D. Kang, C. Wu and X. Tu (2021). "A Review of Non-Thermal Plasma Technology: A novel solution for CO2 conversion and utilization." Renewable & sustainable energy reviews **135**: 109702.
Ghassemi, A. and G. Suresh Kumar (2007). "Changes in fracture aperture and fluid pressure due to thermal stress and silica dissolution/precipitation induced by heat extraction from subsurface rocks." Geothermics **36**(2): 115-140.
Ghassemi, A. and Q. Zhang (2006). "Porothermoelastic Analysis of the Response of a Stationary Crack Using the Displacement Discontinuity Method." Journal of engineering mechanics **132**(1): 26-33.
Hao, Z., H. Fei, Q. Hao and L. Liu (2015). "China First Discovered Massive Available Hot Dry Rock Resources." Acta geologica Sinica (Beijing) **89**(3): 1039-1040.
Hofmann, H., G. Blöcher, H. Milsch, T. Babadagli and G. Zimmermann (2016). "Transmissivity of aligned and displaced tensile fractures in granitic rocks during cyclic loading." International journal of rock mechanics and mining sciences (Oxford, England : 1997) **87**: 69-84.
Huang, Y., Y. Zhang, X. Gao, Y. Ma and Z. Hu (2021). "Experimental and numerical investigation of seepage and heat transfer in rough single fracture for thermal reservoir." Geothermics **95**: 102163.
Li, K., B. Pan and R. Horne (2015). "Evaluating fractures in rocks from geothermal reservoirs using resistivity at different frequencies." Energy (Oxford) **93**(P1): 1230-1238.

Liu, R., B. Li and Y. Jiang (2016). "Critical hydraulic gradient for nonlinear flow through rock fracture networks: The roles of aperture, surface roughness, and number of intersections." Advances in water resources **88**: 53-65.
Lu, S.-M. (2018). "A global review of enhanced geothermal system (EGS)." Renewable & sustainable energy reviews **81**: 2902-2921.
Olasolo, P., M. C. Juárez, M. P. Morales, S. D´Amico and I. A. Liarte (2016). "Enhanced geothermal systems (EGS): A review." Renewable and Sustainable Energy Reviews **56**: 133-144.
Peng, H., Z. Zhao, W. Chen, Y. Chen, J. Fang and B. Li (2020). "Thermal effect on permeability in a single granite fracture: Experiment and theoretical model." International journal of rock mechanics and mining sciences (Oxford, England : 1997) **131**: 104358.
Polak, A., D. Elsworth, H. Yasuhara, A. S. Grader and P. M. Halleck (2003). "Permeability reduction of a natural fracture under net dissolution by hydrothermal fluids." Geophysical research letters **30**(20): 2020-n/a.
Rabczuk, T. and T. Belytschko (2004). "Cracking particles: a simplified meshfree method for arbitrary evolving cracks." International Journal for Numerical Methods in Engineering **61**(13): 2316-2343.
Shu, B., R. Zhu, D. Elsworth, J. Dick, S. Liu, J. Tan and S. Zhang (2020). "Effect of temperature and confining pressure on the evolution of hydraulic and heat transfer properties of geothermal fracture in granite." Applied energy **272**: 115290.
Shu, B., R. Zhu, J. Tan, S. Zhang and M. Liang (2019). "Evolution of permeability in a single granite fracture at high temperature." Fuel (Guildford) **242**: 12-22.
Siratovich, P. A., M. C. Villeneuve, J. W. Cole, B. M. Kennedy and F. Bégué (2015). "Saturated heating and quenching of three crustal rocks and implications for thermal stimulation of permeability in geothermal reservoirs." International journal of rock mechanics and mining sciences (Oxford, England : 1997) **80**: 265-280.
Usman, M., K. Khalid and M. A. Mehdi (2021). "What determines environmental deficit in Asia? Embossing the role of renewable and non-renewable energy utilization." Renewable energy **168**: 1165-1176.
Vogler, D., F. Amann, P. Bayer and D. Elsworth (2016). "Permeability Evolution in Natural Fractures Subject to Cyclic Loading and Gouge Formation." Rock mechanics and rock engineering **49**(9): 3463-3479.
Watanabe, N., N. Hirano and N. Tsuchiya (2006). Experimental evaluation of fluid flow through artificial shear fracture in Granite.
Watanabe, N., K. Saito, A. Okamoto, K. Nakamura, T. Ishibashi, H. Saishu, T. Komai and N. Tsuchiya (2020). "Stabilizing and enhancing permeability for sustainable and profitable energy extraction from superhot geothermal environments." Applied energy **260**: 114306.
Witherspoon, P. A., J. S. Y. Wang, K. Iwai and J. E. Gale (1980). "Validity of Cubic Law for fluid flow in a deformable rock fracture." Water resources research **16**(6): 1016-1024.
Xu, T., Y. Yuan, X. Jia, Y. Lei, S. Li, B. Feng, Z. Hou and Z. Jiang (2018). "Prospects of power generation from an enhanced geothermal system by water circulation through two horizontal wells: A case study in the Gonghe Basin, Qinghai Province, China." Energy (Oxford) **148**: 196-207.
Yasuhara, H. and D. Elsworth (2008). "Compaction of a Rock Fracture Moderated by Competing Roles of Stress Corrosion and Pressure Solution." Pure and applied geophysics **165**(7): 1289-1306.
Yasuhara, H., D. Elsworth and A. Polak (2004). "Evolution of permeability in a natural fracture: Significant role of pressure solution." Journal of Geophysical Research: Solid Earth **109**(B3): B03204-n/a.
Yasuhara, H., N. Kinoshita, H. Ohfuji, D. S. Lee, S. Nakashima and K. Kishida (2011). "Temporal alteration of fracture permeability in granite under hydrothermal conditions and its interpretation by coupled chemo-mechanical model." Applied geochemistry **26**(12): 2074-2088.
Yasuhara, H., A. Polak, Y. Mitani, A. S. Grader, P. M. Halleck and D. Elsworth (2006). "Evolution of fracture permeability through fluid–rock reaction under hydrothermal conditions." Earth and planetary science letters **244**(1): 186-200.
Yuan, Y., T. Xu, J. Moore, H. Lei and B. Feng (2020). "Coupled Thermo-Hydro-Mechanical Modeling of Hydro-Shearing Stimulation in an Enhanced Geothermal System in the Raft River Geothermal Field, USA." Rock mechanics and rock engineering **53**(12): 5371-5388.
Zhang, C., S. Hu, S. Zhang, S. Li, L. Zhang, Y. Kong, Y. Zuo, R. Song, G. Jiang and Z. Wang (2020). "Radiogenic heat production variations in the Gonghe basin, northeastern Tibetan Plateau: Implications for the origin of high-temperature geothermal resources." Renewable energy **148**: 284-297.
Zhao, Y., C. L. Wang and J. Bi (2020). "Analysis of Fractured Rock Permeability Evolution Under Unloading Conditions by the Model of Elastoplastic Contact Between Rough Surfaces." Rock mechanics and rock engineering **53**(12): 5795-5808.
Zhong, C., T. Xu, Y. Yuan, B. Feng and H. Yu (2022). "The feasibility of clean power generation from a novel dual-vertical-well enhanced geothermal system (EGS): A case study in the Gonghe Basin, China." Journal of Cleaner Production **344**: 131109.
Zhou, S., X. Zhuang and T. Rabczuk (2018). "A phase-field modeling approach of fracture propagation in poroelastic media." Engineering Geology **240**: 189-203.
Zhou, X.-P., G.-Q. Li and H.-C. Ma (2020). "Real-time experiment investigations on the coupled thermomechanical and cracking behaviors in granite containing three pre-existing fissures." Engineering fracture mechanics **224**: 106797.
Zimmerman, R. W. and G. S. Bodvarsson (1996). "Hydraulic conductivity of rock fractures." Transport in porous media **23**(1): 1-30.